Water Research 183 (2020) 116095

Contents lists available at ScienceDirect

Water Research

journal homepage: www.elsevier.com/locate/watres

TiO_2 microspheres with cross-linked cyclodextrin coating exhibit improved stability and sustained photocatalytic degradation of bisphenol A in secondary effluent

Esmeralda García-Díaz [a], Danning Zhang [b, c], Yilin Li [d], Rafael Verduzco [b, d, *], Pedro J.J. Alvarez [b, c, **]

[a] Centre of Chemistry, Science Institute, Benemérita Universidad Autónoma de Puebla, Ciudad Universitaria, Edif. IC7, Puebla, Pue, 72570, Mexico
[b] Nanosystems Engineering Research Center for Nanotechnology Enabled Water Treatment (NEWT), United States
[c] Department of Civil & Environmental Engineering, Houston, TX, 77005, United States
[d] Department of Chemical and Biomolecular Engineering, Rice University, Houston, TX, 77005, United States

ARTICLE INFO

Article history:
Received 25 March 2020
Received in revised form
10 June 2020
Accepted 20 June 2020
Available online 28 June 2020

Keywords:
β-cyclodextrin
Fluorinated polymer
Photocatalysis
Decorated TiO_2

ABSTRACT

Photocatalytic water treatment has significant potential to disinfect and degrade recalcitrant organic pollutants while minimizing the need to add chemicals, but current approaches have poor energy efficiency due, in part, to inefficient utilization of photo-generated reactive oxygen species (ROS). Organic coatings such as cyclodextrin (CD) can adsorb target contaminants and bring them close to the photocatalyst surface to enhance ROS utilization efficiency, but the coatings themselves are susceptible to ROS attack. Here, we report an ROS-resistant fluorinated CD polymer (CDP) that can both adsorb contaminants and resist degradation by ROS, yielding a more efficient material for "trap and zap" water treatment. We produced the CDP through condensation polymerization of β-cyclodextrin and tetrafluoroterephthalonitrile, resulting in a cross-linked, covalently bound CD film that is much more stable than prior approaches involving physi-sorption. We optimized the coating thickness on TiO_2 microspheres to improve the efficiency of contaminant degradation, and found that increasing the CDP content enhanced BPA adsorption but also occluded photocatalytic sites and hindered photocatalytic degradation. The optimum content of CDP was 5% by weight, and this optimal CDP-TiO_2 composition had a BPA adsorption capacity of 36.9 ± 1.0 mg g^{-1} compared with 24.1 ± 1.1 mg g^{-1} for CD-coated TiO_2 (CD-TiO_2) and 21.9 ± 1.5 mg g^{-1} for bare TiO_2. CDP-TiO_2 exhibited minimal photoactivity loss after 1000 h of repeated use in DI water under UVA irradiation (365 nm, 3.83 × 10^{-6} E $L^{-1}s^{-1}$), and no release of organic carbon from the coating was detected. Photocatalytic treatment using CDP-TiO_2 only showed a small decrease in BPA removal efficiency in secondary effluent after four 3-h cycles, from 80.2% to 71.7%. In contrast, CD-TiO_2 and P25 removed only 29.8% and 6.2% of BPA after 4 cycles, respectively. Altogether, the CDP-TiO_2 microspheres represent promising materials for potential use in photocatalytic water treatment.

1. Introduction

Photocatalytic water treatment has significant potential to disinfect and degrade a wide variety of recalcitrant organic pollutants while minimizing the need to add chemicals (Loeb et al., 2019; Xu et al., 2014). However, current photocatalytic water treatment processes have low energy efficiency due to low quantum yield, poor utilization of photo-generated reactive oxygen species (ROS), and high energy requirements to recover suspended photocatalysts by high pressure filtration (Lado Ribeiro et al., 2019;

* Corresponding author. Nanosystems Engineering Research Center for Nanotechnology-Enabled Water Treatment (NEWT), Rice University, Houston, TX, United States.
** Corresponding author. Nanosystems Engineering Research Center for Nanotechnology-Enabled Water Treatment (NEWT), Rice University, Houston, TX, United States.
E-mail addresses: rafaelv@rice.edu (R. Verduzco), alvarez@rice.edu (P.J.J. Alvarez).

https://doi.org/10.1016/j.watres.2020.116095
0043-1354/

Wang et al., 2020). To overcome these limitations, we previously developed micron-sized TiO_2 hierarchical spheres and decorated them with cyclodextrin (CD-TiO_2). The large size (3–5 μm) of the particles facilitated low-energy recovery by low-pressure microfiltration, and we showed that cyclodextrin (CD) was an effective coating that could sorb micropollutants close to the photocatalytic sites, enabling an efficient "trap and zap" strategy (Zhang et al., 2018). Other examples of "trap and zap" photocatalytic materials for water treatment include TiO_2 modified with chelating ligands (Makarova et al., 2000), and carbon based nanocomposites (e.g., molecularly-imprinted graphitic carbon nitride (Yuan et al., 2020), graphene (Zhang et al., 2010), zeolite (Noorjahan et al., 2004), and porous electronspun fibers (Lee et al., 2018).

These examples along with our prior work demonstrate that concentrating target contaminants near ROS-generating sites improves the utilization of ROS, mitigating performance inhibition by co-occurring ROS-scavenging species. However, the CD-TiO_2 particles previously reported had limited durability. Specifically, significant loss of activity was observed after 400 h of use (under 3.64×10^{-6} E $L^{-1}s^{-1}$, $\lambda = 365$ nm) due to ROS-attack on cyclodextrin (Zhang et al., 2018). This underscored the need to develop ROS-resistant surface coatings that do not significantly hinder light penetration (for successful activation) and are able to concentrate target pollutants close to photocatalytic sites.

Fluorine containing polymers tend to be chemically stable and relatively unreactive compared to their non-fluorinated counterparts (Cho and Choi, 2001; Patterson et al., 2014), and their durability as a photostable material has been demonstrated (García et al., 2006). Furthermore, cross-linked polymeric coatings have been proven to exhibit superior stability compared to single-stranded polymers or small molecules as coating substances (Beltrán et al., 2016; Zhou et al., 2016). Therefore, we hypothesized that cyclodextrin crosslinked with fluorinated polymers would be effective for trapping moderately hydrophobic pollutants, and be resistant to ROS attack.

Here, we report hierarchical TiO_2 microspheres coated with a cross-linked, fluorine-containing β-cyclodextrin polymers (CDP-TiO_2). Micron-sized TiO_2 hierarchical spheres were utilized as photocatalysts because they are composed of an earth abundant material, and are amenable for low-cost separation process and reuse (e.g., by low-pressure filtration). We describe the preparation of these microspheres, demonstrate their effectiveness in the uptake and degradation of bisphenol A (BPA), and study their performance under multiple and long-term photodegradation studies. The performance of CDP-TiO_2 was benchmarked against CD-TiO_2 and commercial TiO_2 (Evonik P25) for photocatalytic removal of BPA in a secondary effluent polishing context. The stability of anchored CDP was evaluated by monitoring total organic carbon (TOC) released in CDP-TiO_2 dispersion during continuous irradiation, and the long-term performance of CDP-TiO_2 was assessed and compared to CD-TiO_2 under similar conditions.

2. Materials and methods

2.1. Chemicals

Tetrafluoroterephthalonitrile (≥99%), K_2CO_3 (≥99%), anhydrous tetrahydrofuran (THF, ≥99.9%), Titanium isopropoxide ($Ti(OCH(CH_3)_2)_4$,TIP, ≥97%), P25 (≥99.5%), triethanolamine (≥99%), diethanolamine (≥99%), cyanamide (≥99%), β-cyclodextrin (≥99%), N,N-dimethylformamide (DMF, ≥99.8%), bisphenol A (BPA,≥99%), KH_2PO_4 (≥99%), Hydrochloric acid (36.5%), Acetonitrile (≥99%) were purchased from Sigma Aldrich.

2.2. Synthesis of β-cyclodextrin polymer (CDP)

The synthesis of CDP followed a modified procedure previously reported (Alsbaiee et al., 2016). Briefly, β-cyclodextrin (600 mg, 0.53 mmol), tetrafluoroterephthalonitrile (300 mg, 1.5 mmol) and K_2CO_3 (900 mg, 6.5 mmol) were dispersed in anhydrous THF (12 mL) and degassed with nitrogen. The solution was sealed in a pressure vessel and heated at 85 °C under constant stirring for 48 h. The orange suspension was cooled down naturally and then transferred into 1 M HCl to remove excessive K_2CO_3. The pale-yellow products were filtered out using 0.22 μm PTFE syringe filter, washed thoroughly with ethanol and DI water, and dried under vacuum at 60 °C overnight. Yield: 56 wt %.

2.3. Synthesis of bare TiO_2 microsphere and CDP-TiO_2

The synthesis of the of TiO_2 microspheres followed the methodology previously reported by Zhang (Zhang et al., 2018). TiO_2 microspheres were fabricated via a hydrothermal method with TIP as the precursor. In detail, 1.2 mL of TIP was added dropwise into a well-mixed triethanolamine (20 mL) and DMF (10 mL) solution. The mixture was constantly stirred for 30 min, transferred into a 50 mL Teflon-lined stainless-steel autoclave, and heated at 200 °C for 24 h. The products were collected by centrifugation and calcined under 550 °C to remove remaining impurities. Next, CDP was anchored onto the as-prepared TiO_2 microspheres. CDP (50 mg), TiO_2 microspheres (200 mg) and 200 μL of cyanamide (50% aqueous solution) were dispersed in 25 mL buffered water (0.1 M phosphate, pH = 6). The mixture was then refluxed under 90 °C in oil bath for 8 h. The product was collected and washed with water thoroughly to remove impurities.

2.4. Characterization of CDP-TiO_2 materials

The morphology of CDP-TiO_2 materials was observed by scanning field emission electron microscope (FE-SEM, TESCAN) at 10 kV. FTIR (Fourier transform infrared spectra) was obtained preparing a KBr tablet and scanning from 4000 to 400 cm^{-1} in a Nicolet iS50 Thermo Scientific instrument. Thermogravimetric analysis (TGA) was performed on SDT Q600 (TA Instruments) at a heating rate of 10 °C/min from room temperature to 700 °C with a flowing air gas stream of 50 mL min^{-1}. The materials were analyzed by measuring the N_2 adsorption isotherms at −196 °C using the surface analyzer instrument Autosorb-3B, Quantachrome. The samples were degassed at 100 °C during 12 h before the analysis. The specific surface area was calculated using the Brunauer–Emmett–Teller (BET) equation, and the pore size distribution was calculated using the Barret–Joyner–Halenda (BJH) method.

2.5. BPA adsorption tests

The catalyst (20 mg) was dispersed into 40 mL solution with an initial BPA concentration of 20 mg L^{-1}. Aliquots (200 μL) were taken at predetermined time intervals, and the remaining BPA in the solution was analyzed to obtain the adsorption kinetics.

The BPA concentration was determined by HPLC (LC-20AT, Shimadzu) chromatography equipped with a UV–vis detector. A dC18 reverse-phase column (Atlantis, 3 μm, 3.9 × 15 mm, Waters), was used for separation with acetonitrile – water (60:40; v:v) at a flow rate of 1 mL min^{-1}. The detection and quantification limits of BPA analysis were 1 and 10 μg L^{-1} respectively. The amount of BPA adsorbed was calculated using the equation: $q_e = (C_i - C_e)V/m$, where q_e is the adsorbate amount adsorbed on the adsorbent at equilibrium (mg g^{-1}), C_i is the initial concentration in water (mg L^{-1}), C_e is the final equilibrium concentration in water (mg L^{-1}), V is

the solution volume (L), and m is the mass of the adsorbent (g). To characterize adsorption kinetics, time course data were fit to a *pseudo*-second order kinetic model, which considers a two-step adsorption process involving solute diffusion through the adsorbent and then chemical sorption as the rate-limiting step (Ho and McKay, 1999). Adsorption of solutes to complex materials with abundant and diverse adsorption sites tends to follow *pseudo*-second order kinetics (Wang and Guo, 2020), where the rate of change in the amount adsorbed (dq/dt) is proportional to the squared difference between the equilibrium adsorption capacity (q_e) and the amount adsorbed at any time (q):

$$\frac{dq}{dt} = k_2(q_e - q)^2 \quad (1)$$

where k_2 is the adsorption rate constant. Eq. (1) can be integrated to:

$$q = \left(q_e^2 k_2 t\right) \Big/ (1 + q_e k_2 t) \quad (2)$$

The catalyst (20 mg) was dispersed into 40 mL solution with various initial BPA concentration (10–200 mg L^{-1}) for adsorption isotherm test. The equilibrium concentration of BPA was analyzed after 24 h.

2.6. Photocatalytic degradation of BPA and evaluation on catalyst stability

The photocatalytic activity of the CDP-TiO_2 was tested in a batch system with Six UVA lamps (365 nm, 4 W, F4T5/BLB) irradiation. The photon flux was 3.83×10^{-6} E $L^{-1}s^{-1}$ measured by actinometry (Bolton et al., 2011). UVA light (365 nm) was used for irradiation, considering that higher-energy UVC (which is primarily used for disinfection) is easily absorbed by organics – resulting in inefficient utilization and potential deterioration of some materials (Phong and Hur, 2016). The catalyst (20 mg) was dispersed into 40 mL BPA solution (20 mg L^{-1}) in a quartz beaker. Although higher BPA concentrations have been reported in some industrial effluent (Chou et al., 2014; Lee et al., 2015), this initial BPA concentration is relatively high compared to those commonly found in municipal secondary effluent, which rarely exceed a few μg L^{-1} (Hu et al., 2019; Spataro et al., 2019). Nevertheless, it facilitated chemical analysis to characterize sorption and degradation processes, and served to demonstrate proof-of-concept under more challenging treatment conditions (i.e., relatively high BPA concentrations) (Ahmed et al., 2011; Saadati et al., 2016). Aliquots (1 mL) were taken after predetermined intervals of irradiation time, and the catalysts were filtered out using 0.22 μm PTFE syringe filter. Photocatalytic degradation tests of BPA were conducted in the context of deionized water or a secondary effluent polishing from a treatment plant. The performance of CDP-TiO_2 was benchmarked against P25 in secondary effluent for four treatment cycles (3 h per cycle). After each cycle the solid was separated by centrifugation.

Photocatalysis by-products were identified by HPLC-MS, in a MicroToF (Bruker) equipped with an ESI source and interfaced with an Agilent 1200 HPLC. A C18 column (Imtakt, Sherzo SM-C18, 3 μm, 150 mm × 2 mm) was used for separation with acetonitrile/water (both buffered with 0.1% of formic acid) as the mobile phase. A gradient method was applied to mobile phase; started with 2% acetonitrile and maintained for 5 min, then increased the ratio of acetonitrile to 50% in 10 min and maintained for 10 min, and decreased to 2% acetonitrile in 5 min.

The potential destruction of CDP coating after repeated usage was determined by measuring the total organic carbon (TOC) in the CDP-TiO_2 material dispersion after 100 h irradiation under the same conditions as the photocatalysis experiments. The catalyst was separated by centrifugation and the TOC was measured by TOC-VCHS (Shimadzu). The stability of CDP-TiO_2 was evaluated through repeated usage for 1000 h. In detail, 20 mg of CDP-TiO_2 was dispersed into 40 mL of BPA (20 mg L^{-1}) solution and kept irradiation for 1000 h. The catalyst was collected by centrifugation at specific time intervals (i.e. 100, 200, 400, 600, 800, and 1000 h) to evaluate its long-term performance on BPA removal.

3. Results and discussion

3.1. Preparation of cross-linked, fluorinated cyclodextrin polymer coating with resistance to ROS oxidation

We prepared a fluorinated, cross-linked CD polymer (CDP) coating anchored to the surface of TiO_2 microspheres to enable contaminant sorption near photocatalytic sites and improve stability in the presence of ROS. The CDP coating was prepared though condensation polymerization of β-cyclodextrin and tetrafluoroterephthalonitrile, as previously reported (Alsbaiee et al., 2016), although we prepared it in a relatively simple batch reaction step. Separately, TiO_2 microsphere photocatalysts were prepared via a hydrothermal method, as previously reported (Zhang et al., 2018). To anchor the CDP onto the TiO_2 microsphere surface, the CDP and TiO_2 were dispersed in water in the presence of cyanamide. The resulting materials were washed extensively to remove unattached CDP. This general procedure enables us to tune the amount of CDP coating present on the TiO_2 microspheres, and we prepared CDP-TiO_2 microspheres with varying amounts of CDP coatings. The materials were labeled according to the weight percentage of CDP anchored: CDP(3%)-TiO_2, CDP(5%)-TiO_2 and CDP(30%)-TiO_2, as determined by thermogravimetric analysis (TGA).

The resulting CDP-TiO_2 particles were characterized in terms of morphology, surface chemistry, and pore structure. The SEM images of CDP(5%)-TiO_2 (Fig. 1a) showed a hierarchichally structured surface and constituent nanosheets. The diameter of CDP(5%)-TiO_2 was in the range of 3–5 μm. Successful anchoring of CDP was confirmed through FTIR analysis (Fig. 1b). Three bands at 2929 cm^{-1}, 1157 cm^{-1}, and 1029 cm^{-1} were identified from the spectra of CDP-TiO_2 which represent C–H stretch, C–O stretch of cyclodextrin and the O–C–O antisymmetric glycosidic vibrational modes respectively (Wang et al., 2019). The signals observed at 1320, 1484, and 1675 cm^{-1} correspond to C–F stretch, C–C aromatic stretch and C=N nitrile stretch, respectively.

CDP(5%)-TiO_2 had a BET surface area of 197.2 m^2 g^{-1} which was three times higher than commercial TiO_2 (Evonik, P25) (58.9 m^2 g^{-1}, Table S1). The specific surface decreased as the content of CDP increased (Table S1). This was expected because the specific area of CDP (3.8 m^2 g^{-1}) is much lower than that for bare TiO_2 microspheres (208.9 m^2 g^{-1}). The CDP-TiO_2 has similar textural characteristics to bare TiO_2 microspheres, both having the same isotherm and hysteresis loop type and an average pore size between 3 and 11 nm (Fig. S1 and Table S1). The nitrogen adsorption isotherms for these particles are of type II (Fig. 1d), which indicates the formation of nonporous or macroporous structure (Thommes et al., 2015).

3.2. Improved BPA adsorption capacity after CDP anchoring relative to bare and cyclodextrin-coated TiO_2 microspheres

Next, we studied the potential for the CDP nanoparticles to uptake BPA in water through adsorption tests. Compared with bare TiO_2 microspheres and CD-TiO_2, CDP coating significantly enhanced the BPA adsorption rate and capacity, and this is reflected in the adsorption kinetics data (Fig. 2a). The *pseudo*-second order model

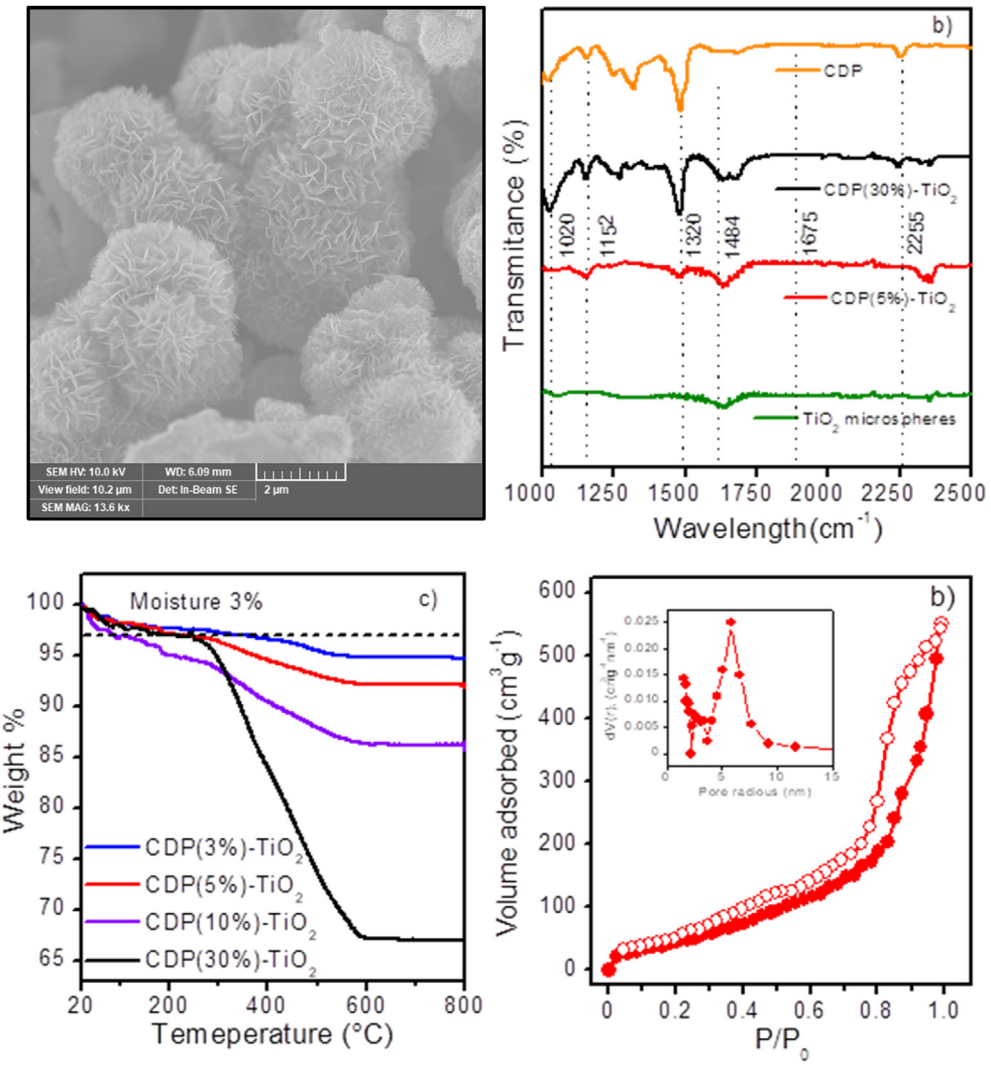

Fig. 1. Characterization of CDP-TiO_2, CDP, and bare TiO_2 microspheres. a) SEM images of CDP(5%)-TiO_2 particles (3–5 µm). b) FTIR spectra for CDP(30%)-TiO_2, CDP(5%)-TiO_2, CDP, and bare TiO_2 microspheres. c) Thermogravimetric analysis of CDP-TiO_2 with varying CDP content (3%, 5%, 10% and 30% wt.). d) Nitrogen adsorption isotherm and pore size distribution for CDP(5%)-TiO_2 (specific surface area of 197.2 m^2 g^{-1}).

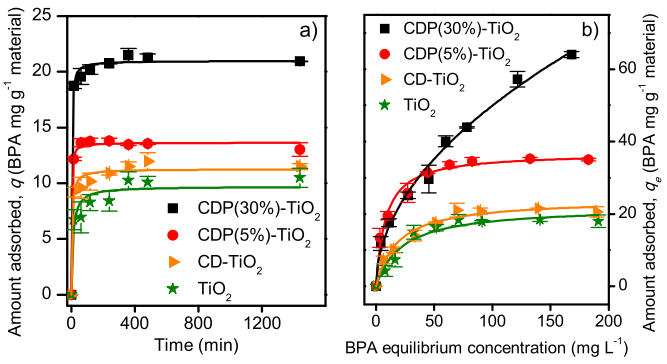

Fig. 2. a) Adsorption kinetics and b) adsorption isotherms of BPA onto bare TiO_2 microspheres, CD-TiO_2 and CDP-TiO_2. CDP coating improved both the adsorption rate and capacity.

produced an excellent fit of the adsorption kinetics data (Equation (2)). This fit was superior than that from a *pseudo*-first order kinetics model, based on Pearson's chi-squared test (Fig. S2a and S2b). The second-order model parameters for each microsphere tested are provided in Table S2, and show that the adsorption rate of CDP(5%)-TiO_2 was two times higher than that of CD-TiO_2 and four times higher than that of bare TiO_2 microspheres (Table S2). The adsorption isotherms also showed that the adsorption capacity increased with increasing content of CDP (Fig. 2b), even though the specific surface area decreased as the content of coated CDP increased (Table S1).

The adsorption isotherm for all microspheres exhibited a plateau above 50 mg g^{-1}, with the exception of CDP(30%)-TiO_2 in which the amount of BPA adsorbed increased monotonically up to the highest concentration tested (200 mg g^{-1}). The adsorption isotherm of the CDP(30%)-TiO_2 material were best fit by the Freundlich model, in which the adsorption capacity increase exponentially with the initial concentration. In contrast, all other materials followed the Langmuir model (Al-Ghouti and Da'ana, 2020). This likely reflects a shift from monolayered adsorption pattern (described by the Langmuir isotherm) to multi-layered adsorption (described by the Freundlich isotherm), consistent with the apparent formation of multi-layer CDP coating on the TiO_2 surface when increasing CDP loading. The adsorption parameters

are shown in Table 1 and show that the CDP-TiO_2 microspheres have higher adsorption capacities than bare TiO_2 or CD-TiO_2 microspheres.

3.3. Enhanced photocatalytic degradation of BPA after CDP coating relative to bare and cyclodextrin-coated TiO_2 microspheres

Next, we tested the effectiveness of CDP-TiO_2 for the photocatalytic degradation of BPA. Photocatalytic degradation of BPA was tested with different catalysts in DI water to evaluate the effect of CDP coating on photoactivity without confounding effects by background ROS scavengers (Fig. S3). The photocatalytic degradation data followed pseudo first order kinetics (Fig. S3). The rate constant for BPA degradation (Table S3) by CDP(5%)-TiO_2 (0.025 ± 0.002) min^{-1} was 1.7 times higher than that for bare TiO_2 microspheres (0.015 ± 0.001) min^{-1}, and similar to that previously reported for CD-TiO_2 (0.025 ± 0.001 min^{-1}) (Zhang et al., 2018).

Next, we tested the performance of the microspheres in the presence of competing species. Effluent organic matter (EfOM) is present in secondary effluent and competes with BPA for CDP sorption sites, occludes the photocatalytic surface and scavenges photogenerated ROS. Photocatalytic degradation tests on BPA with CDP-TiO_2 were conducted in secondary effluent (TOC = 8.64 ± 0.25 mg L^{-1}, pH = 7.2) from a local wastewater treatment plant (69th St. Wastewater treatment complex of Houston, TX) (Fig. 3). While CDP-TiO_2 particles removed 99.8% of BPA within 2 h when tested in DI water, only 80.2% of BPA was degraded after 3 h treatment in secondary effluent. In addition, CDP(5%)-TiO_2 showed progressive loss of photoactivity in cycling tests in secondary effluent, with BPA removal decreasing to 71.7% by the fourth cycle. Nevertheless, this decrease in performance was not as significant as observed for either CD-TiO_2 or P25, which removed only 29.8% and 6.2% BPA by the fourth cycle in secondary effluent, respectively (Fig. 3). These results demonstrate that CDP-TiO_2 is less susceptible to inhibition by competing species compared with CD-TiO_2 or P25. We attribute this to the greater adsorption rate and capacity for these nanoparticles. Additionally, P25 readily aggregates in the presence of multivalent ions such as Ca^{2+} (Katz et al., 2015), and the average particle size (Table S4) increased from 300 ± 4 nm (in DI water) to 800 ± 12 nm (in secondary effluent), which leads to decreased surface area and photoactivity. In contrast, aggregation of CDP-TiO_2 was insignificant (Zhang et al., 2018; Zhao et al., 2018); the average particle size of CDP-TiO_2 in either DI water (Tables S4, 3.62 ± 0.4 μm) or in secondary effluent (3.89 ± 0.6 μm) determined by DLS was statistically undistinguishable, and similar to the SEM observation (3–5 μm).

TiO_2 microspheres with various amounts of CDP coating were tested in DI water to optimize the extent of surface modification (Fig. 4a). BPA adsorption increased with CDP content, but the rate constants of photocatalytic degradation of BPA exhibited a bell-shaped pattern as a function of CDP content (Fig. 4b). Specifically, photocatalytic degradation rate increased with polymer content (up to 5%). The degradation rate constant k was 0.023 ± 0.001 min^{-1} for CDP(3%)-TiO_2 and 0.025 ± 0.002 min^{-1} for CDP(5%)-TiO_2.

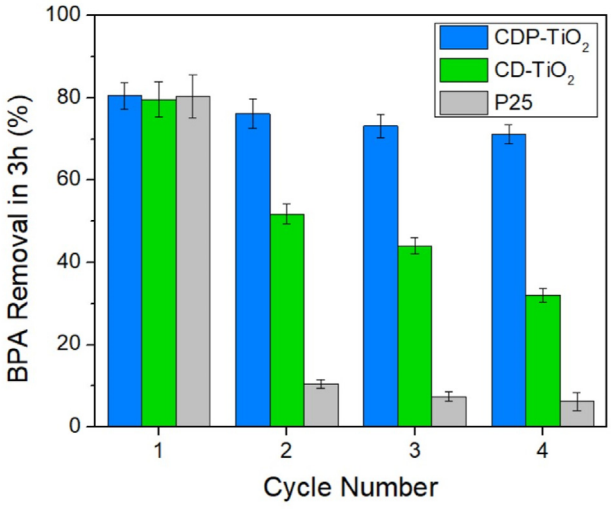

Fig. 3. CDP-TiO_2 outcompeted CD-TiO_2 and P25 during photocatalytic degradation of BPA in a secondary effluent polishing context monitored over four cycles. CDP-TiO_2 was less inhibited by interfering constituents in secondary effluent compared to CD-TiO_2 and P25 [benchmarking data from our previous work conducted under identical conditions (Zhang et al. (2018)]. The initial BPA concentration was 20 mg L^{-1} each cycle.

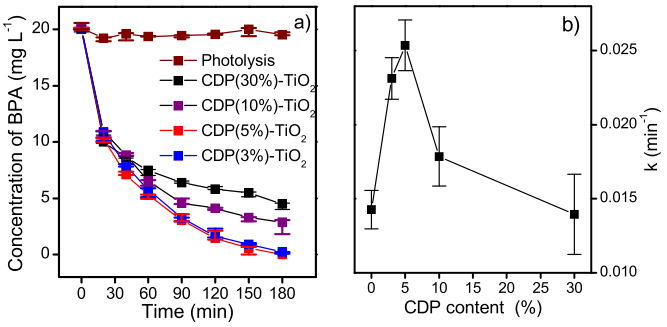

Fig. 4. Influence of CDP content on BPA removal (a) and photocatalytic rate constant (b) in DI water. Increasing CDP content is initially beneficial due to enhanced BPA "trapping", but excessive coating occludes photocatalytic sites and hinders BPA "zapping". The optimum content of CDP was 5% weight in this system.

However, further increases in the CDP content had a detrimental effect on BPA degradation efficiency. The degradation rate constant for CDP(30%)-TiO_2 was 0.014 ± 0.003 min^{-1}. We attribute this increase in degradation rate followed by a decrease at higher CDP contents to an increase in adsorption capacity with increasing CDP but also higher probability for occlusion of photocatalytic sites on the TiO_2 surface by the polymer. Furthermore, CDP is fluorescent under UVA irradiation (Fig. S4) and may compete with the TiO_2 surface for photons.

Table 1
Parameters used to model adsorption isotherms for CD-TiO_2 and CDP-TiO_2 particles. q_m (mg g^{-1}) is the maximum adsorption capacity (mg g^{-1}), and K_L (L mg^{-1}) is the constant related to the free energy of adsorption. K_F ($mg^{1-(1/n)}$ $L^{1/n}$ g^{-1}) is a constant indicative of the relative adsorption capacity of the adsorbent and n is the dimensionless constant related with the intensity of the adsorption.

	Langmuir	K_L (L mg^{-1})	q_m (mg g^{-1})	χ^2	R^2
Bare TiO_2 microsphere	$q_e = \frac{q_m K_L C_e}{1 + K_L C_e}$	0.045 ± 0.01	21.9 ± 1.5	2.30	0.9837
CD-TiO_2		0.055 ± 0.01	24.1 ± 1.1	1.49	0.9738
CDP(5%)-TiO_2		0.124 ± 0.02	36.9 ± 1.0	2.45	0.9836
	Freundlich	K_F ($mg^{1-(1/n)}$ $L^{1/n}$ g^{-1})	n		
CDP(30%)- TiO_2	$q_e = K_F C_e^{1/n}$	4.89 ± 0.58	1.98 ± 0.10	4.0	0.9910

Based on ion chromatographic analysis (Fig. S5), the production of radicals •OH was the primary mechanism to destroy BPA by photocatalysis, leading to the formation of the hydroxylated compounds showed in Table S5. The most abundant compound was the BPA-O-catechol formed from the addition of an •OH group onto the aromatic ring of the BPA. The identified compounds from the ion chromatograph shown in Fig. S5 coincide with some byproducts reported in the Fenton process (Molkenthin et al., 2013; Mu et al., 2017; Yang et al., 2016; Zhang et al., 2014; Zheng et al., 2018).

3.4. Stability considerations

The CDP coating was significantly more stable than the baseline CD coating previously reported (Zhang et al., 2018). We monitored the stability of CDP(5%)-TiO_2 nanoparticles under irradiation in clean DI water by measuring the TOC (0.55 ± 0.01 mg L^{-1}), and only 2.4 % wt. Of the CDP coating was released as dissolved TOC after 100 h of irradiation.

Photocatalytic durability was enhanced compared with CD-TiO_2, which after 500 h of irradiation experienced 70% degradation or detachment of CD (Zhang et al., 2018). The CDP(5%)-TiO_2 photocatalytic nanoparticles remained stable and active under long-term irradiation. No significant loss of photoactivity was observed after 1000 h. The rate constant decreased slightly from 0.027 ± 0.002 min^{-1} for unexposed CDP(5%)-TiO_2 to 0.024 ± 0.001 min^{-1} for CDP(5%)-TiO_2 (Fig. 5). In contrast, significant loss of activity was observed for CD-TiO_2 after 400 h usage. These results demonstrate significant photocatalytic stability for CDP-TiO_2 nanoparticles, providing a potential route to more practical photocatalytic applications.

4. Conclusions

A novel ROS-resistant fluorinated cyclodextrin polymer was used as a coating for TiO_2 microspheres and provided superior photoactivity and durability, benchmarked against CD-TiO_2 and commercial P25. The CDP-TiO_2 microspheres are promising multifunctional catalysts for advanced water treatment that enable a "trap-and-zap" treatment approach and are more resistant than P25 TiO_2 to interference by background constituents in a secondary effluent polishing context. Furthermore, the coated CDP microspheres exhibit minor photoactivity loss after 1000 h of continuous use, whereas, significant loss of activity was observed for CD-TiO_2 after 400 h usage under similar conditions. Finally, the size of the CDP-TiO_2 enables separation by low-pressure filtration (and thus resulting in low energy requirements). Altogether, the CDP-TiO_2 microspheres represent promising materials for potential use in photocatalytic water treatment and secondary effluent polishing.

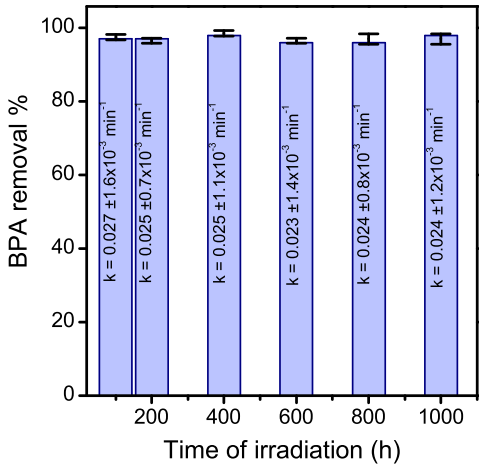

Fig. 5. Stability of CDP(5%)-TiO_2 after continuous usage up to 1000 h under the irradiation at $\lambda = 365$ nm and 3.83×10^{-6} E $L^{-1}s^{-1}$. Cross-linking cyclodextrin with fluorinated polymer is highly resistant to ROS attack that insignificant loss of photoactivity was observed after 1000 h of use. The initial BPA concentration was 20 mg L^{-1} each cycle.

Declaration of competing interest

The authors declare that they have no known competing financial interests or personal relationships that could have appeared to influence the work reported in this paper.

Acknowledgments

This research is supported by the NSF ERC on Nanotechnology-Enabled Water Treatment (EEC-1449500). One of the authors (EG) was also supported by COMEXUS through a Fulbright- García Robles grant.

Appendix A. Supplementary data

Supplementary data to this article can be found online at https://doi.org/10.1016/j.watres.2020.116095.

References

Ahmed, S., Rasul, M.G., Martens, W.N., Brown, R., Hashib, M.A., 2011. Advances in heterogeneous photocatalytic degradation of phenols and dyes in wastewater: a review. Water Air Soil Pollut. 215, 3–29. https://doi.org/10.1007/s11270-010-0456-3.

Al-Ghouti, M.A., Da'ana, D.A., 2020. Guidelines for the use and interpretation of adsorption isotherm models: a review. J. Hazard Mater. 393, 122383. https://doi.org/10.1016/J.JHAZMAT.2020.122383.

Alsbaiee, A., Smith, B.J., Xiao, L., Ling, Y., Helbling, D.E., Dichtel, W.R., 2016. Rapid removal of organic micropollutants from water by a porous β-cyclodextrin polymer. Nature 529, 190–194. https://doi.org/10.1038/nature16185.

Beltrán, A., Mikhailov, M., Sokolov, M.N., Pérez-Laguna, V., Rezusta, A., Revillo, M.J., Galindo, F., 2016. A photobleaching resistant polymer supported hexanuclear molybdenum iodide cluster for photocatalytic oxygenations and photodynamic inactivation of: Staphylococcus aureus. J. Mater. Chem. B 4, 5975–5979. https://doi.org/10.1039/c6tb01966h.

Bolton, J.R., Stefan, M.I., Shaw, P.S., Lykke, K.R., 2011. Determination of the quantum yields of the potassium ferrioxalate and potassium iodide-iodate actinometers and a method for the calibration of radiometer detectors. J. Photochem. Photobiol. A Chem. 222, 166–169. https://doi.org/10.1016/j.jphotochem.2011.05.017.

Cho, S., Choi, W., 2001. Solid-phase photocatalytic degradation of PVC–TiO_2 polymer composites. J. Photochem. Photobiol. A Chem. 143, 221–228. https://doi.org/10.1016/S1010-6030(01)00499-3.

Chou, P.H., Liu, T.C., Lin, Y.L., 2014. Monitoring of xenobiotic ligands for human estrogen receptor and aryl hydrocarbon receptor in industrial wastewater effluents. J. Hazard Mater. 277, 13–19. https://doi.org/10.1016/j.jhazmat.2014.02.049.

García, O., Sastre, R., del Agua, D., Costela, A., García-Moreno, I., 2006. New fluorinated polymers doped with BODIPY chromophore as highly efficient and photostable optical materials. Chem. Mater. 18, 601–602. https://doi.org/10.1021/cm052027t.

Ho, Y.S., McKay, G., 1999. Pseudo-second order model for sorption processes. Process Biochem. 34, 451–465. https://doi.org/10.1016/S0032-9592(98)00112-5.

Hu, Y., Zhu, Q., Yan, X., Liao, C., Jiang, G., 2019. Occurrence, fate and risk assessment of BPA and its substituents in wastewater treatment plant: a review. Environ. Res. 178 https://doi.org/10.1016/j.envres.2019.108732.

Katz, A., McDonagh, A., Tijing, L., Shon, H.K., 2015. Fouling and inactivation of titanium dioxide-based photocatalytic systems. Crit. Rev. Environ. Sci. Technol. 45, 1880–1915. https://doi.org/10.1080/10643389.2014.1000763.

Lado Ribeiro, A.R., Moreira, N.F.F., Li Puma, G., Silva, A.M.T., 2019. Impact of water matrix on the removal of micropollutants by advanced oxidation technologies. Chem. Eng. J. 363, 155–173. https://doi.org/10.1016/j.cej.2019.01.080.

Lee, C.G., Javed, H., Zhang, D., Kim, J.H., Westerhoff, P., Li, Q., Alvarez, P.J.J., 2018. Porous electrospun fibers embedding TiO_2 for adsorption and photocatalytic degradation of water pollutants. Environ. Sci. Technol. 52, 4285–4293. https://doi.org/10.1021/acs.est.7b06508.

Lee, S., Liao, C., Song, G.J., Ra, K., Kannan, K., Moon, H.B., 2015. Emission of bisphenol analogues including bisphenol A and bisphenol F from wastewater treatment plants in Korea. Chemosphere 119, 1000–1006. https://doi.org/10.1016/j.chemosphere.2014.09.011.

Loeb, S.K., Alvarez, P.J.J., Brame, J.A., Cates, E.L., Choi, W., Crittenden, J., Dionysiou, D.D., Li, Q., Li-Puma, G., Quan, X., Sedlak, D.L., David Waite, T., Westerhoff, P., Kim, J.H., 2019. The technology horizon for photocatalytic water treatment: sunrise or sunset? Environ. Sci. Technol. 53, 2937–2947. https://doi.org/10.1021/acs.est.8b05041.

Makarova, O.V., Rajh, T., Thurnauer, M.C., Martin, A., Kemme, P.A., Cropek, D., 2000. Surface modification of TiO_2 nanoparticles for photochemical reduction of nitrobenzene. Environ. Sci. Technol. 34, 4797–4803. https://doi.org/10.1021/es001109+.

Molkenthin, M., Olmez-Hanci, T., Jekel, M.R., Arslan-Alaton, I., 2013. Photo-Fenton-like treatment of BPA: effect of UV light source and water matrix on toxicity and transformation products. Water Res. 47, 5052–5064. https://doi.org/10.1016/j.watres.2013.05.051.

Mu, C., Zhang, Y., Cui, W., Liang, Y., Zhu, Y., 2017. Removal of bisphenol A over a separation free 3D Ag_3PO_4-graphene hydrogel via an adsorption-photocatalysis synergy. Appl. Catal. B Environ. 212, 41–49. https://doi.org/10.1016/j.apcatb.2017.04.018.

Noorjahan, M., Kumari, V.D., Subrahmanyam, M., Boule, P., 2004. A novel and efficient photocatalyst: TiO_2-HZSM-5 combinate thin film. Appl. Catal. B Environ. 47, 209–213. https://doi.org/10.1016/j.apcatb.2003.08.004.

Patterson, R., Kandelbauer, A., Müller, U., Lammer, H., 2014. 17 - crosslinked thermoplastics. In: Dodiuk, H., Goodman, S.H. (Eds.), Handbook of Thermoset Plastics, third ed. William Andrew Publishing, Boston, pp. 697–737. https://doi.org/10.1016/B978-1-4557-3107-7.00017-8.

Phong, D.D., Hur, J., 2016. Non-catalytic and catalytic degradation of effluent dissolved organic matter under UVA-and UVC-irradiation tracked by advanced spectroscopic tools. Water Res. 105, 199–208. https://doi.org/10.1016/j.watres.2016.08.068.

Saadati, F., Keramati, N., Ghazi, M.M., 2016. Influence of parameters on the photocatalytic degradation of tetracycline in wastewater: a review. Crit. Rev. Environ. Sci. Technol. 46 (8), 757–782. https://doi.org/10.1080/10643389.2016.1159093.

Spataro, F., Ademollo, N., Pescatore, T., Rauseo, J., Patrolecco, L., 2019. Antibiotic residues and endocrine disrupting compounds in municipal wastewater treatment plants in Rome, Italy. Microchem. J. 148, 634–642. https://doi.org/10.1016/j.microc.2019.05.053.

Thommes, M., Kaneko, K., Neimark, A.V., Olivier, J.P., Rodriguez-Reinoso, F., Rouquerol, J., Sing, K.S.W., 2015. Physisorption of gases, with special reference to the evaluation of surface area and pore size distribution (IUPAC Technical Report). Pure Appl. Chem. 87, 1051–1069. https://doi.org/10.1515/pac-2014-1117.

Wang, H., Liu, Z. hua, Zhang, J., Huang, R.P., Yin, H., Dang, Z., 2020. Human exposure of bisphenol A and its analogues: understandings from human urinary excretion data and wastewater-based epidemiology. Environ. Sci. Pollut. Res. 27, 3247–3256. https://doi.org/10.1007/s11356-019-07111-9.

Wang, J., Guo, X., 2020. Adsorption kinetic models: physical meanings, applications, and solving methods. J. Hazard Mater. 390, 122156. https://doi.org/10.1016/j.jhazmat.2020.122156.

Wang, L., Zhang, Q., Chen, B., Bu, Y., Chen, Y., Ma, J., Rosario-Ortiz, F.L., Zhu, R., 2020. Some issues limiting photo(cata)lysis application in water pollutant control: a critical review from chemistry perspectives. Water Res. 174, 115605. https://doi.org/10.1016/J.WATRES.2020.115605.

Wang, Z., Cui, F., Pan, Y., Hou, L., Zhang, B., Li, Y., Zhu, L., 2019. Hierarchically micro-mesoporous β-cyclodextrin polymers used for ultrafast removal of micro-pollutants from water. Carbohydr. Polym. 213, 352–360. https://doi.org/10.1016/j.carbpol.2019.03.021.

Xu, H., Ouyang, S., Liu, L., Reunchan, P., Umezawa, N., Ye, J., 2014. Recent advances in TiO_2-based photocatalysis. J. Mater. Chem. A 2, 12642–12661. https://doi.org/10.1039/c4ta00941j.

Yang, X., Xu, X., Xu, X., Xu, J., Wang, H., Semiat, R., Han, Y., 2016. Modeling and kinetics study of Bisphenol A (BPA) degradation over an $FeOCl/SiO_2$ Fenton-like catalyst. Catal. Today 276, 85–96. https://doi.org/10.1016/j.cattod.2016.01.002.

Yuan, Q., Zhang, D., Yu, P., Sun, R., Javed, H., Wu, G., Alvarez, J.J.P., 2020. Selective adsorption and photocatalytic degradation of extracellular antibiotic resistance genes by molecularly-imprinted graphitic carbon nitride. Environ. Sci. Technol. 54 (7), 4621–4630. https://doi.org/10.1021/acs.est.9b06926.

Zhang, D., Lee, C., Javed, H., Yu, P., Kim, J.H., Alvarez, P.J.J., 2018. Easily recoverable, micrometer-sized TiO_2 hierarchical spheres decorated with cyclodextrin for enhanced photocatalytic degradation of organic micropollutants. Environ. Sci. Technol. 52, 12402–12411. https://doi.org/10.1021/acs.est.8b04301.

Zhang, X., Ding, Y., Tang, H., Han, X., Zhu, L., Wang, N., 2014. Degradation of bisphenol A by hydrogen peroxide activated with $CuFeO_2$ microparticles as a heterogeneous Fenton-like catalyst: efficiency, stability and mechanism. Chem. Eng. J. 236, 251–262. https://doi.org/10.1016/j.cej.2013.09.051.

Zhang, Y., Tang, Z.-R., Fu, X., Xu, Y.-J., 2010. TiO_2 graphene nanocomposites for gas-phase photocatalytic degradation of volatile aromatic pollutant: is. ACS Nano 4, 7303–7314. https://doi.org/10.1021/nn1024219.

Zhao, X., Du, P., Cai, Z., Wang, T., Fu, J., Liu, W., 2018. Photocatalysis of bisphenol A by an easy-settling titania/titanate composite: effects of water chemistry factors, degradation pathway and theoretical calculation. Environ. Pollut. 232, 580–590. https://doi.org/10.1016/j.envpol.2017.09.094.

Zheng, X., Xu, S., Wang, Y., Sun, X., Gao, Y., Gao, B., 2018. Enhanced degradation of ciprofloxacin by graphitized mesoporous carbon (GMC)-TiO_2 nanocomposite: strong synergy of adsorption-photocatalysis and antibiotics degradation mechanism. J. Colloid Interface Sci. 527, 202–213. https://doi.org/10.1016/j.jcis.2018.05.054.

Zhou, W., Cao, Y., Sui, D., Guan, W., Lu, C., Xie, J., 2016. Ultrastable BSA-capped gold nanoclusters with a polymer-like shielding layer against reactive oxygen species in living cells. Nanoscale 8, 9614–9620. https://doi.org/10.1039/C6NR02178F.